Diffuse light tomography to detect blood vessels using Tikhonov regularization

Huseyin Ozgur Kazanci*[a], Steven L. Jacques[b]
[a] Biomedical Engineering, Faculty of Engineering, Akdeniz University, 07058 Antalya, TURKEY;
[b]Biomedical Engineering and Dermatology Oregon Health & Science University, CH13B 3303 SW Bond Avenue, Portland, OR 97239

ABSTRACT

Detection of blood vessels within light-scattering tissues involves detection of subtle shadows as blood absorbs light. These shadows are diffuse but measurable by a set of source-detector pairs in a spatial array of sources and detectors on the tissue surface. The measured shadows can reconstruct the internal position(s) of blood vessels. Continuous wave diffuse optical tomography (CWDOT) method is used to detect the bloody vessels inside the tissue. Imaging device has back-reflection geometry sources and detectors on the surface. From each source position laser light is sent into tissue, back reflected photons are collected by photo-sensitive photo-detectors. The tomographic method involves a set of N_s sources and N_d detectors such that $N_{sd} = N_s \times N_d$ source-detector pairs produce N_{sd} measurements, each interrogating the tissue with a unique perspective, i.e., a unique region of sensitivity to voxels within the tissue. This tutorial report describes the reconstruction of the image of a blood vessel within a soft tissue based on such source-detector measurements, by solving a matrix equation using Tikhonov regularization. This is not a novel contribution, but rather a simple introduction to a well-known method, demonstrating its use in mapping blood perfusion.

Keywords: Diffuse optical tomography, diffuse light tomography, inverse problem solution, Tikhonov regularization, monte carlo simulation, biomedical optic, diffuse optic imaging, laser imaging.

1. INTRODUCTION

1.1 Experimental imager

Consider an imager consisting of 50 source fibers and 50 detector fibers that is placed on the tissue surface, inter-mixed as shown in Fig. 1 in a grid pattern with 1.2-mm spacings. There are 50 x 50 = 2500 possible source-detector pairs, N_{sd} = 2500, allowing 2500 measurements of light transport through the tissue, observed as escaping flux per unit surface area and referred to here as

$$r(i) = \sqrt{(x_s(i) - x_d(i))^2 + (y_s(i) - y_d(i))^2} \quad (1)$$

R(i) [cm^{-2}], i = [1:N_{sd}], at locations $x_s(i)$, $y_s(i)$, $x_d(i)$, $y_d(i)$, with source-detector separations.

Back reflection continuous wave diffuse optical tomography (CWDOT) imaging device with 50 sources and 50 detectors on the surface of it has been thought and realize for imaging medium. Source and detector separations and neighborhoods of all source and detector couplings have been defined and distances have been computed and grouped. For each source and detector couplings, 2 dimensional (2D) Monte Carlo (MC) simulations for photon-tissue interactions have been done, respectively. In Fig. 1 source and detector placements have been shown. Generated 2D MC data has been transferred from 2D MC simulation code composition through 3D image reconstruction platform. Transfer process could be done by different methods such as weight matrix translational method which was presented detailed[1]. 2D MC simulations of photon-tissue interactions base on the Rytov or Born approximation of diffusion equation of nuclear radiative transport equation, respectively. The particle nature of photon transport in tissue is basically used. Scattering and absorption events by the effect of computer random number photon probability density function is essential parameters for MC simulation of photon-tissue interaction events. Basically, 2D MC simulation for specific optical properties of imaging tissue has been run then generated pencil beam cylindrical photon fluence rate distributions have been transferred through 3D image reconstruction environment, respectively.

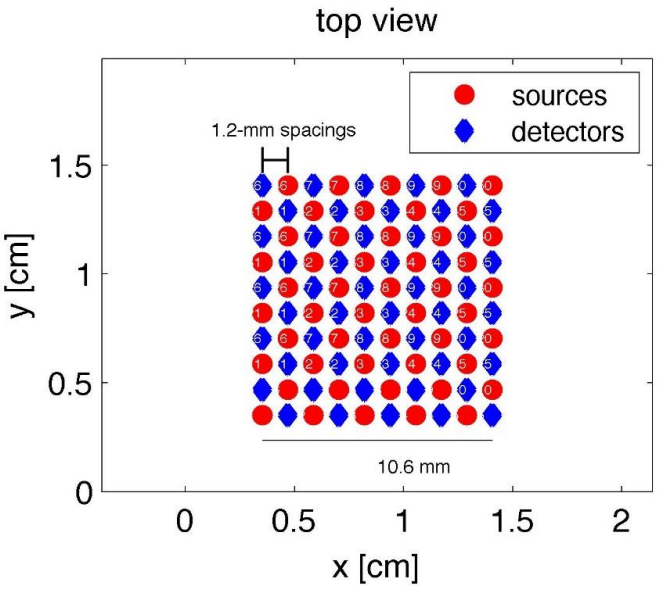


Figure 1. Top view of the positions of 50 source fibers and 50 detector fibers on the surface of a tissue. The grid covers 10.8 mm x 10.8 mm

2. MATERIALS AND METHODS

2.1 Background tissue properties and light transport

The light transport is defined in [1] for homogeneous background tissue. This set of N_{sd} measurements R(i) can specify the background tissue optical properties by assuming the tissue is a homogeneous medium and ignoring the very slight perturbations caused by any blood vessels in the tissue. The background optical properties of the tissue are

absorption coefficient μ_{a0} [cm^{-1}]

reduced scattering coefficient μ_{s0}' [cm^{-1}]

The distance between each source and detector, r(i), and the measurements R(i) are analyzed by least squares fitting, using a transport theory function, getRr(), predicted

$$pR(i) = getRr(\mu_{a0}, \mu_{s0}', r(i), n) \quad (2)$$

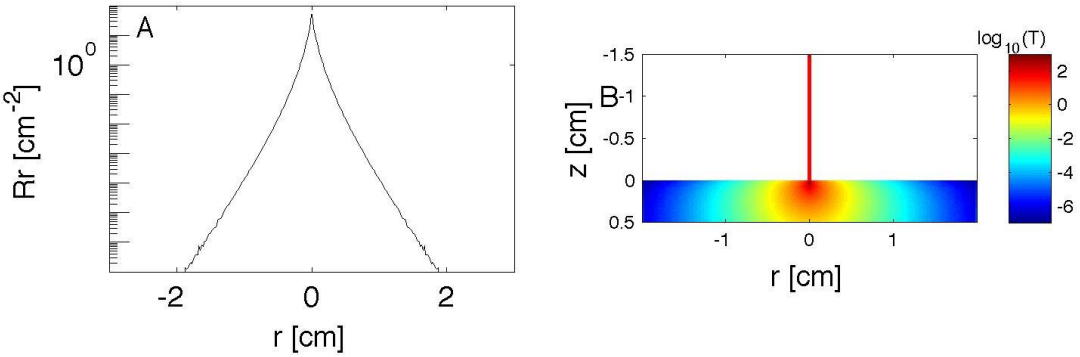


Figure 2**.** Monte Carlo simulation of light transport in tissue. (A) Escaping flux at surface, R(r) [cm^{-2}]. (B) Relative fluence rate, ϕ [W/cm^2 per W delivered], which is called transport T [$1/cm^2$]

Where n is the refractive index mismatch at the tissue surface, eg., 1.4/1.0. This transport theory function can be based on simple diffusion theory or it can be a lookup table based on Monte Carlo simulations, which is preferable when evaluating the transport between closely spaced source-detector pairs[3-8]. Figure 2 shows the Monte Carlo simulation of light transport for the background medium, created by the MCML program, which is used in this example.

The least squares fitting iteratively improves its guess of the optical properties of absorption coefficient μ_{a0} and reduced scattering coefficient μ_{s0}', until the predicted pR(i) of the theory match the experimental R(i).

Figure 3A illustrates the R(i) versus r(i) data (Monte Carlo generated), fit by theory (Monte Carlo) (yes, of course the fit is perfect). Also the fluence rate $\phi(z=0,r)$ is shown, indicating the relation between R(r) and $\phi(0,r)$. Figure 3B shows the ratio $\phi(0,r)/R(r)$ versus r. Therefore, measurements of R(i) can be converted to fluence at the surface at the detector fiber, $\phi(0,r)$ = R(i) x ratio, before running the tomographic algorithm.

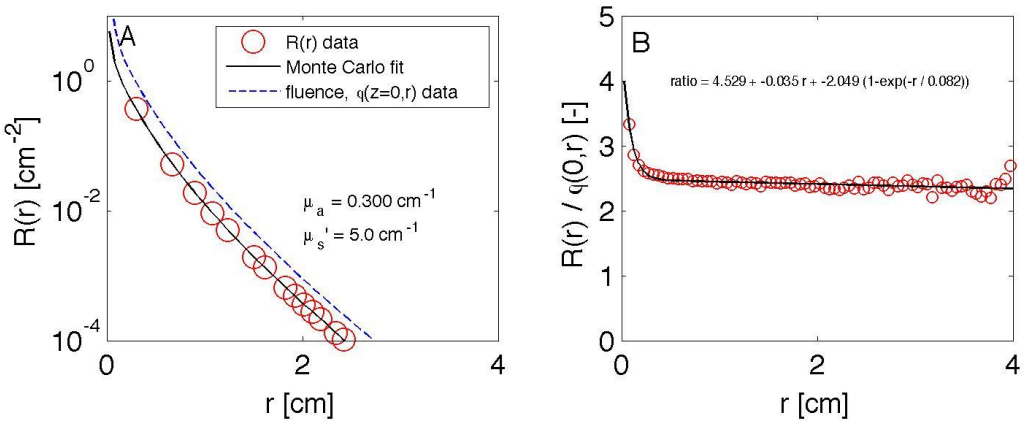


Figure 3. Monte Carlo simulation of measurements. **(A)** R(r) [cm^{-2}] for imager. Several source-detector measurements have the same spacing r. Black line is theory fit to the data. The Monte Carlo used μ_a = 0.841 cm^{-1}, μ_s = 171 cm^{-1}, and g = 0.90, so μ_s' = 17.1 cm^{-1}. Refractive index mismatch at surface was 1.4. **(B)** The ratio $\varphi_{surface}$ / R versus r. (Ignores the collection efficiency of the fiber, usually around 0.10-0.20, instead using all the escaping flux to define R(r))

While all the details of this step to define the background optical properties are not discussed here, hopefully the idea is clear. For this tutorial report, the background tissue properties are: μ_{a0} = 0.841 [cm^{-1}], μ_{s0} = 171 [cm^{-1}], g = 0.90, μ_{s0}' = 17.1 [cm^{-1}] which are typical values for a tissue at wavelengths in the near-IR wavelength range. The experimental measurements R(i) are analyzed by a homogeneous tissue model to yield the background tissue optical properties, the optical properties are used to predict the surface fluence rate Φ_0 of the background tissue, the R(i) are converted to the surface fluence rate Φ(i) at the detector of each source-detector-pair measurement.

2.2 Blood absorption within a vessel

A key factor in the problem of detecting a vessel is knowing the absorption of light by blood within the vessel. A strong absorption will give the vessel contrast relative to background tissue. This example uses 585 nm wavelength light. At 585 nm, the absorption coefficient of blood at 97% oxygenation is 164.4 cm^{-1}. The scattering properties are similar to the background soft tissue. This example uses a field of view of 2 cm divided into 20 voxels. The equal-sided voxels have a width of w = 2 cm/20 voxels = 0.1 cm, and a volume of $V = w^3 = 1x10^{-3}$ cm^3. Consider a blood vessel of diameter d whose cross-sectional area matches the cross-sectional area of one voxel, $\pi d^2/4 = w^2$, or $d = 2w/\sqrt{\pi} = 0.1128$ cm ≈ 1.13 mm. Therefore, a 1.13-mm-dia. blood vessel is here modeled as one row of 1-mm-wide voxels along the y dimension at one position, x, y.

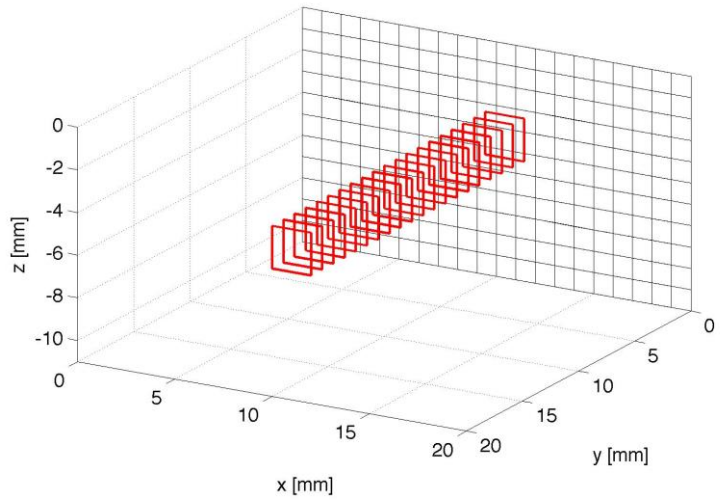


Figure 4. App. 1.13-mm-dia. blood vessel by a row of 1-mm-wide voxels. Cross-sectional areas of vessel & voxel are equal

2.3 Monte Carlo simulations of sensitivity to voxel perturbation

Using the Monte Carlo simulation in Fig. 2, the transport of light from a source fiber to a voxel within the tissue and from that voxel to a detector is calculated.

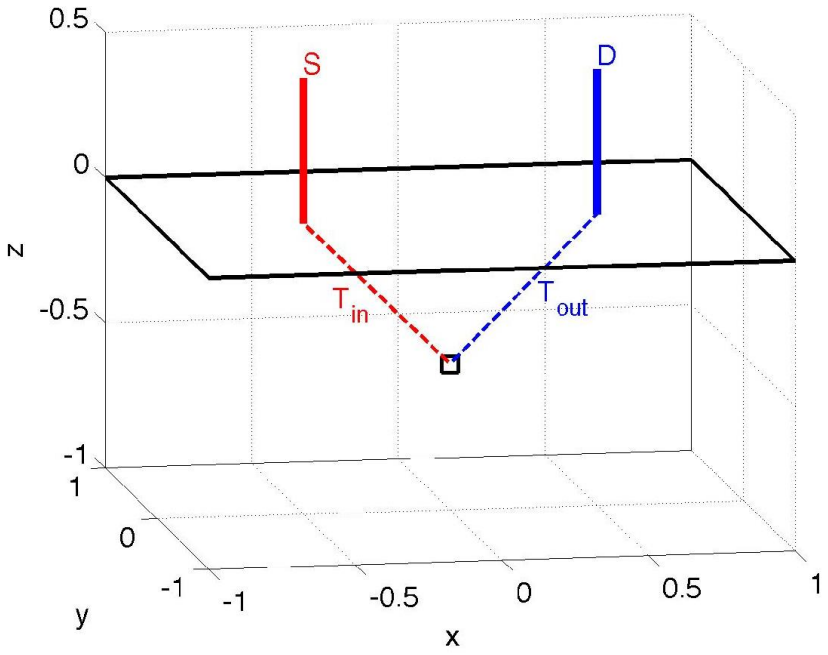


Figure 5. Light transport from a source fiber to a voxel within the tissue and from that voxel to a detector

The transport of light from a source fiber to a voxel at x, y, z is called T_{in} [cm^{-2}]. The transport of light from a voxel at x, y, z to a detector fiber is called T_{out} [cm^{-2}]. The incremental absorption $\Delta\mu_a$ [cm^{-1}] in voxels corresponding to the 1.13-mm-dia. blood vessel is $\Delta\mu_a = \mu_{a.blood} - \mu_{a0} = 164.4 - 0.841 = 163.6$ cm^{-1}. The perturbation that is caused by the $\Delta\mu_a$ [cm^{-1}] in each voxel is equal to the product $-T_{in}T_{out}\Delta\mu_a V$ [cm^{-2}], in units of transport. The perturbation is negative if $\Delta\mu_a$ is positive because absorption removes light from the light field (and positive if $\Delta\mu_a$ is negative). Consequently, the transport measured by a particular source-detector pair is:

$$\Phi = \Phi_0 - T_{in}T_{out}\Delta\mu_a V \quad (3)$$

$T_{in}T_{out}$ constitutes the map of "sensitivity" of a measurement to a perturbing absorption in each voxel. Figure 4 shows maps of the $T_{in}T_{out}$ [cm^{-4}] for one particular source-detector pair (top view and side view).

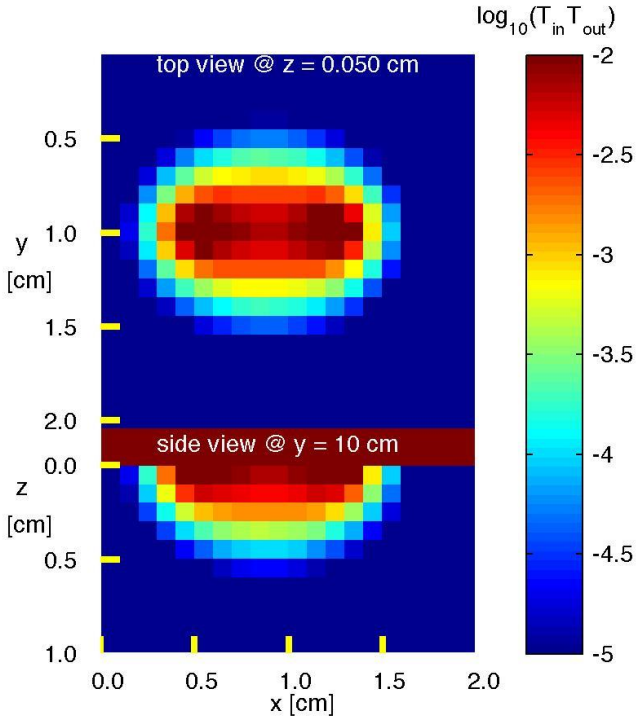


Figure 6. The map of sensitivity TinTout [cm-4] for one example of a particular source-detector pair. (TOP) Top view, @surface. (BOTTOM) Side view, @y = 2.0 cm

The tissue volume is divided into a set of voxels, with N_x bins along the x-axis, N_y bins along the y-axis, and N_z bins along the z-axis. In this example, N_x = 20 bins, N_y = 20 bins, N_z = 10 bins, for a total of $N_v = N_x*N_y*N_z$ = 4000 voxels. The matrix solution described below requires 11.5 s on a 2.7 GHz processor using MATLAB™. If the number of voxels is much larger than 4000, the time required for the matrix solution becomes prohibitively long. A set of N_{sd} maps of $T_{in}T_{out}$ (like Fig. 4) is constructed, which are reshaped as a matrix $T_{in}T_{out}(j,k)$, where j = 1: N_{sd}, k=1: N_v. The observed escaping flux (R) collected by each detector fiber is related to the transport signal (T) reaching the detector fiber at the surface. The relationship between T and R is a constant that depends on the refractive index mismatch at the tissue surface and the numerical aperture of the detector fiber. For this tutorial, we will work with the T that reaches the detector fiber, i.e., an "observed" T, rather than citing an experimental R. (The relationship between T and R was discussed above.) The difference between the background T_0 and the experimental T for each source-detector pair is called ΔT. A matrix M equals $T_{in}T_{out}V$, where V is the voxel volume V = dx*dy*dz. The parameter to be determined is the perturbing $\Delta\mu_a$. In summary, the parameters to be used in the matrix solution are:
$\Delta\Phi = \Phi_0 - \Phi$ (a vertical vector of length N_{sd}), measured "experimentally", i.e., simulation + added 1% noise M = $T_{in}T_{out}V$ (a matrix of size N_{sd}, N_v), based on Monte Carlo simulations $\Delta\mu_a$ (a vertical vector of length N_v), to be calculated as the reconstructed image

2.4. The matrix solution using Tikhonov regularization

The matrix equation is:

$$\Delta\Phi = M \times \Delta\mu_a \quad (4)$$

To solve for P, first multiply both sides of the equation by the transpose of M, M^T,

$$M^T\Delta T = M^T M \times \Delta\mu_a \tag{5}$$

Next, multiply both sides of the equation by the inverse of the product M^TM. The product $(M^TM)^{-1}M^TM$ reduces to an identity matrix, hence the result is now simply $\Delta\mu_a$:

$$(M^TM)^{-1}M^T\Delta T = (M^TM)^{-1}M^TM \times \Delta\mu_a = \Delta\mu_a \tag{6}$$

Therefore, the solution for $\Delta\mu_a$ is

$$\Delta\mu_a = (M^TM)^{-1}M^T\Delta T \tag{7}$$

But this solution is not stable and experiments have always noisy data. There is a need for a slight addition of value along the diagonal of product matrix $(M^TM)^{-1}M^T$, which has size N_{sd}, N_v. Such an addition is commonly referred to as Tikhonov regularization in[9].

$$\Delta\mu_{a_Tikhonov} = (M^TM + \lambda I)^{-1}M^T\,\Delta T \tag{8}$$

3. RESULTS

In Equation 8, I is an identity matrix of size Nsd, Nv, and λ is a very small value, somewhere in the range of 10-22 to 10-8. If λ is too low, the image breaks up into many positive and negative ghosts, and yields a chaotic image. If λ is too high, the image loses all contrast and no longer shows the vessel. The best λ for each depth position of the vessel was manually chosen as the value which just began to allow slight ghosts to appear. The following plot of best λ versus vessel depth was obtained. Using these best choices of λ, the images of the vessel at different depths were prepared

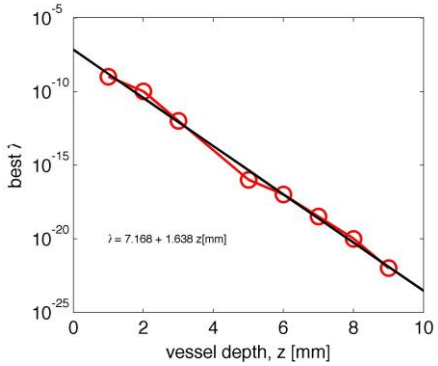


Figure 7. Best choice of λ when placing the vessel at different depths

Using these best choices of λ, the images of the vessel at different depths were prepared:

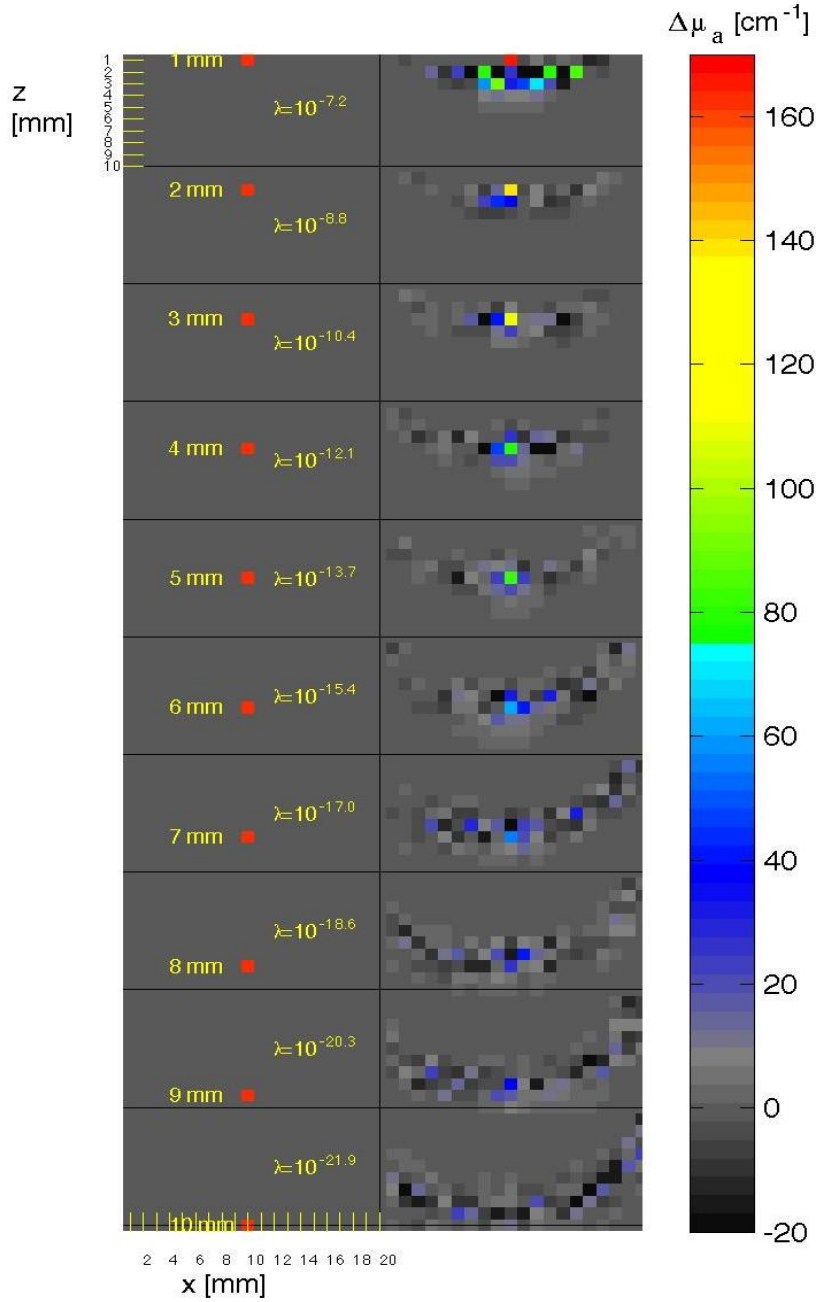


Figure 8. The tomographic reconstruction of a blood vessel at different depths, with **1% noise**. (A) The true perturbing absorption ($\Delta\mu_a$ = 163.6 cm^{-1}) and position of vessel. (B) The reconstructed images

The signal of the reconstructed voxel at the position of the vessel shows a $\Delta\mu_a$ that initially matches the true value (163.6 cm^{-1}) but then drops toward zero as the vessel is placed deeper. In other words, the accuracy of the reconstruction is altered by the depth of the vessel. Figure 7 shows this fall in accuracy:

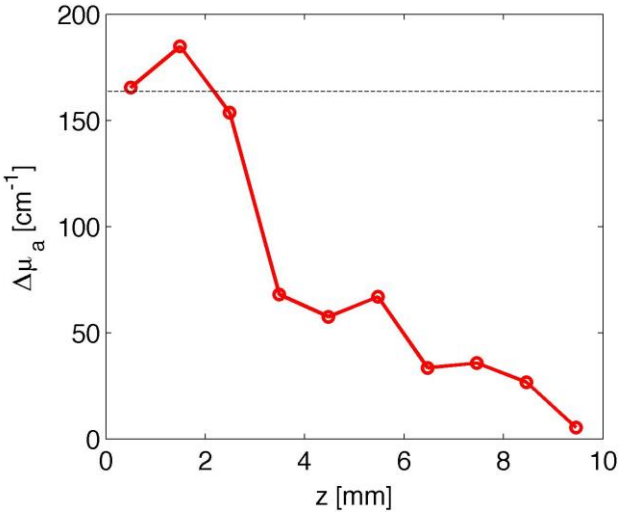


Figure 9. Fall in accuracy of reconstructed $\Delta\mu_a$ when placing the vessel at different depths. Dashed horizontal line indicates the true $\Delta\mu_a$ of blood vessel (163.6 cm^{-1})

One can correct for this systematic fall in accuracy (assuming it is systematic), but eventually at depths beyond ~6 mm the signal falls to the level of the residual ghosts, so the contrast between the vessel and surrounding tissue would not be improved. In this example, 6 mm approximately equals 4δ, where δ is the 1/e penetration depth in the background tissue,

$$\delta = \frac{1}{\sqrt{3\mu_{a0}(\mu_{a0} + \mu_{s0}(1-g))}} \tag{9}$$

4. CONCLUSION

In summary, this example of 3D reconstruction uses a 50 source x 50 detector imager and Tikhonov regularization to image a blood vessel. The method requires a very good signal-to-noise ratio (SNR), and in this example a 100:1 SNR is used. The imager can image a 1.13-mm-dia. blood vessel down to 6 mm within a soft tissue using 585-nm-wavelength light, although the accuracy of the absolute value of the reconstructed $\Delta\mu_a$ falls with vessel depth. This report is just an introductory tutorial, designed around a typical optical tomography problem, the detection of a blood vessel. There is a large literature on Tikhonov regularization and tomographic reconstruction in general. It is hoped this introduction might help introduce biomedical optics students to the method, perhaps motivating them to study the topic in more depth.

REFERENCES

[1] Kazanci H.O., "Weight Matrix Analysis for Back Reflection Continuous Wave Diffuse Optical Tomography (CWDOT) systems: Translational Method," Optical and Quantum Electronics, 47(12), 3847-3853, (2015).

[2] Wang, L.V. and Wu, H., [Biomedical Optics Principles and Imaging], John Wiley & Sons, New York, (2007).

[3] Wang, L. and S.L. Jacques, "Optimized radial and angular positions in Monte Carlo modeling," Medical physics, 21(7), 1081-1083, (1994).

[4] Jacques, S.L. and L. Wang, "Monte Carlo modeling of light transport in tissues, in Optical-thermal response of laser-irradiated tissue," Springer. 73-100, (1995).

[5] Wang, L., S.L. Jacques, and L. Zheng, "MCML—Monte Carlo modeling of light transport in multi-layered tissues," Computer methods and programs in biomedicine. 47(2), 131-146, (1995).

[6] Wang, L., S.L. Jacques, and L. Zheng, "Convolution for responses to a finite diameter photon beam incident on multi-layered tissues," Computer methods and programs in biomedicine. 54(3), 141-150, (1997).

[7] Jacques, S.L., "Modeling tissue optics using Monte Carlo modeling: a tutorial," in Biomedical Optics (BiOS). International Society for Optics and Photonics, (2008).

[8] Prahl, S.A., Keijzer M., Jacques S. L., Welc A. J., "A Monte Carlo model of light propagation in tissue," Dosimetry of laser radiation in medicine and biology. 5, 102-111, (1989).

[9] Tikhonov A.N., Arsenin V.L., [Solutions of Ill Posed Problems] V.H. Winston and Sons, New York, (1977).